Eur. Phys. J. D **36**, 165–171 (2005)
DOI: 10.1140/epjd/e2005-00250-2

THE EUROPEAN PHYSICAL JOURNAL D

Strong field dual-pulse excitation of Ag_N

A charge selective analysis of the Coulomb explosion

T. Döppner[a], Th. Fennel, P. Radcliffe[b], J. Tiggesbäumker, and K.-H. Meiwes-Broer

Institut für Physik, Universität Rostock, 18051 Rostock, Germany

Received 27 June 2005 / Received in final form 1st August 2005
Published online 6 September 2005 –

Abstract. The ionization of silver clusters exposed to pairs of intense femtosecond laser pulses strongly depends on the optical delay. Enhanced production of a certain atomic charge state z is obtained by a z-dependent delay. This may open a possible route to control the excitation process and populate specific charge states. The optimum pulse separation which maximizes the generation of highly ionized species varies by more than one order of magnitude when the mean size of the clusters increases from $\overline{N} = 80$ to $\overline{N} = 22000$. Semiclassical Vlasov simulations applied to a model system reveal the importance of the initial ionic motion in the ionization process.

PACS. 36.40.Gk Plasma and collective effects in clusters – 52.50.Jm Plasma production and heating by laser beams (laser-foil, laser-cluster, etc.) – 31.15.Qg Molecular dynamics and other numerical methods

1 Introduction

Experiments on clusters and small particles interacting with strong laser pulses have attracted growing interest because of the observation of highly charged atomic ions [1], energetic particles [2,3] as well as strong emission in the X-ray region of the electromagnetic spectrum [4]. Moreover, measurements by Ditmire et al. have shown that a table-top pulsed neutron source from the strong field exposure of deuterium clusters could be built with a flux which turns out to be comparable to the yield of the Nova Laser experiment, i.e. 10^5 neutrons per Joule of incident laser energy [5]. The nearly complete absorption of strong infrared radiation by a dense cluster target [6] has opened the possibility to build an intense and debris free light source in the soft X-ray regime potentially suitable for EUV-lithography [7–9] and also for time-resolved experiments on biological systems within the water window [10]. Recently, the group of Möller has demonstrated that xenon clusters exposed to intense VUV pulses from the free electron laser at DESY in Hamburg also show an enhanced charging efficiency when compared to single atoms [11]. Due to the different spectral excitation regime other processes compared to the optical region come into play, and the interpretation of the experimental results is a topic of current debate [12,13].

The enhanced absorption of intense optical radiation in nanometer-sized matter results from the coupling to a strongly localized plasma. In rare gas clusters such a nanoplasma can only be generated by an initial ionization through optical field ionization (OFI), whereas in clusters of simple metals it is already present due to electron delocalization [14]. In the latter systems the dominant optical feature is the Mie resonance [15] in which most of the oscillator strength is concentrated [16,17]. However, the energy of the collective electron excitation typically ranges well above the photon energy of a Ti:sapphire laser ($\hbar\omega_L = 1.54\,\mathrm{eV}$). Assuming a simple metallic sphere the plasmon energy

$$\hbar\omega_{Mie} = \hbar\sqrt{\frac{e^2 n_{bg}}{3\epsilon_o m_e}}, \tag{1}$$

depends mainly on the ion density n_{bg}, with the charge e and the mass m_e of the electron, and ϵ_o the dielectric constant. Following that, a matching between the laser frequency and the collective mode can be achieved by a red-shift of the resonance upon an appropriate expansion of the cluster. Therefore, to obtain maximum energy absorption, the laser-cluster interaction can be described as a process consisting of two well-separated steps. First, the initial ionization via OFI triggers the cluster expansion due to Coulomb and hydrodynamic forces leading to a spectral shift of the collective mode. Secondly, a violent coupling is expected when the cluster is irradiated with intense light while the resonance condition is fulfilled. As a result the efficient absorption leads to an extreme charging of the cluster.

[a] e-mail: tilo.doeppner@uni-rostock.de
[b] *Present address*: DESY, Nottke Str. 85, 22607 Hamburg, Germany.

Such a process was first mentioned by Ditmire in his nanoplasma model which describes the response of large rare gas particles to strong laser fields [18]. For metal clusters, which are subject of this contribution, this mechanism was introduced as plasmon enhanced ionization (PLENIO) [19]. Semiclassical Vlasov [20,21] as well as DFT calculations [22] have indeed shown that, when a collective motion of the delocalized electrons is excited, the charging of metal clusters can be strongly enhanced. Moreover, it has been pointed out that the resonant excitation of the collective mode exhibits similarities with the behavior of a classical damped harmonic oscillator driven by the electromagnetic field [23]. We note, that other processes might contribute as well, e.g., ionization ignition (IIM) [24] and enhanced ionization for a certain interatomic distance (ENIO) [25], a mechanism which is well-known from diatomic molecules [26].

Since the ionic motion upon initial charging determines the evolution of the optical properties, the temporal structure of the laser pulse will play a crucial role for the energy absorption. So far mainly the technique of pulse stretching was applied in experiments. By tuning the pulse width the charging [3,19,27] and the X-ray emission [7,8] could be optimized. Recently, these experiments have been extended to dual-pulse excitation, i.e. the pump-probe technique was used to map the dynamics and control the charging [28]. By qualitative comparison with theoretical simulations it was confirmed that the initial ionization can indeed be treated separately from the resonant coupling, according to the plasmon enhanced ionization model.

In this contribution, after the description of the experimental and theoretical methods in Section 2, we will extend the study of reference [28] to a complete analysis of each ionic fragment channel generated in the Coulomb explosion (Sect. 3.1). Several possibilities of data treatment will be presented. In Section 3.2 the dependence of the charging process on the cluster size and on the laser intensity is investigated. When irradiating much larger clusters the optimum delay which generates the highest charge states increases from several hundred femtoseconds by more than one order of magnitude well up into the picosecond regime. In Section 4 the experimental results will be discussed and corroborated by theoretical simulations.

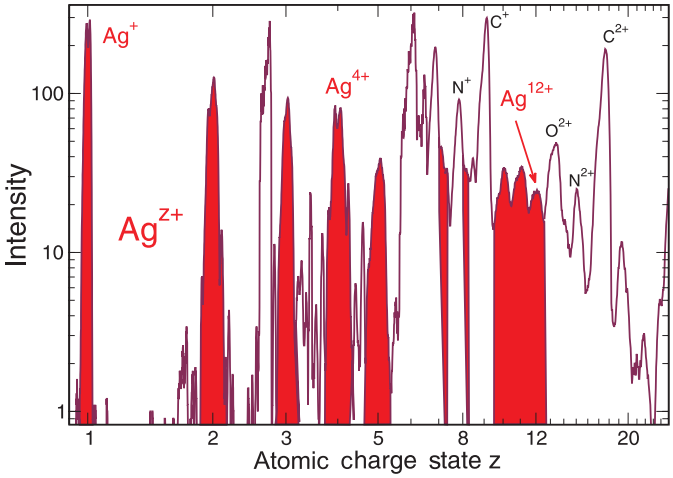

Fig. 1. Charge state distribution of Ag^{z+} after excitation of small silver clusters (mean size $\overline{N} = 80$ atoms) with dual-pulses having an optical delay of 470 fs and a peak intensity of 5.2×10^{15} W/cm^2. Signals of atomic ions resulting from the Coulomb explosion of silver clusters are highlighted. Even though some parts of the mass spectrum are dominated by contributions from residual gas, there are still time channels which can be uniquely assigned to defined charge states z.

2 Methods

2.1 Experimental setup

Silver clusters are produced by gas aggregation of metallic vapor in a magnetron discharge, based on the method first used in the group of Haberland [29]. Details about our source and the experimental setup can be found elsewhere [30]. Briefly, after passing a differential pumping stage the metal clusters are exposed to intense light pulses which traverse perpendicularly to the cluster beam axis. The femtosecond pulses are generated by a Ti:sapphire chirped pulse amplification system typically delivering 25 mJ pulses at 800 nm having a pulse width of 100 fs (FWHM). In the dual-pulse experiments the optical delay is generated by a Mach-Zehnder interferometer setup where the typical energy per pulse is 2.5 mJ. The computer controlled translation stage has a time resolution of 8.3 fs. The laser light is focused by a $f = 1/40$ lens giving intensities of up to 5.2×10^{15} W/cm^2. A variation in laser intensity is usually accomplished by shifting the laser focus with respect to the cluster beam axis. The resulting products of the Coulomb explosion are detected by a reflectron time-of-flight mass spectrometer [31]. Since the recoil energy spectra from the Coulomb explosion of clusters can extend up into the MeV regime [2,30,32] a restriction in energy is necessary in order to achieve a sufficient m/z resolution. In the current setup ions with excess energies larger than $z \times 200$ eV are not collected. Due to this restriction ions with charge states up to $z = 12$ can uniquely be identified, see Figure 1. The resolution of even higher charged ions is prevented due to the background signal from residual gas.

2.2 Vlasov simulations

In order to simulate the time-dependent response of metal clusters exposed to strong optical fields, the Thomas-Fermi-Vlasov molecular dynamics (TFV-MD) is applied. For a detailed description we refer the reader to reference [21]. In brief, TFV-MD treats the electrons semiclassically while the ionic motion is calculated within classical molecular dynamics. As model systems sodium clusters are chosen which are well tested prototypes for simple metal clusters [20,21]. A local pseudopotential is used to describe the interaction between the valence electrons and the ions. Currently, the TFV-MD-simulations are limited

to a single active electron per atom. Hence, no higher charges of the atomic ions can be predicted from the model. However, the scheme provides a detailed qualitative analysis of the main coupling mechanisms. Note that the Vlasov approach is the semiclassical limit of time-dependent density functional calculations [33]. Here we concentrate on the simulation of Na_{55} which, according to the calculations, has a ground state dipole resonance energy of $\hbar\omega_o = 2.84\,\mathrm{eV}$ [21]. The laser pulses are described as linearly polarized dipole fields with a Gaussian pulse envelope having a full width of $\tau = 50\,\mathrm{fs}$, using the experimental photon energy of $\hbar\omega_L = 1.54\,\mathrm{eV}$.

3 Results

3.1 Analysis of dual-pulse signals

For each optical delay a full time-of-flight spectrum as shown in Figure 1 is recorded, typically averaged over 2000 laser shots. In order to analyze a dual-pulse experiment those channels of the spectrum which can be assigned to defined charge states are integrated and plotted with respect to the optical delay. Figure 2 shows results of a dual-pulse experiment on silver clusters which are exposed to laser intensities of up to $5.2\times10^{15}\,\mathrm{W/cm^2}$. The signals of selected multiply charged silver ions (Ag^{z+}) are normalized for better comparison. We note, that the absolute count rate at the maximum of the dual pulse signals decreases roughly exponentially with increasing charge state z. The highest z which can be analyzed in this way with a sufficient statistics is $z_M = 12$. Assuming equal laser pulses and therefore symmetric dual-pulse signals the experimental values are fitted with

$$S(\Delta t) = a_1\left(1 - e^{-a_2|\Delta t|^2}\right)e^{-a_3|\Delta t|} + a_4|\Delta t| + a_5. \quad (2)$$

Such a function turned out to be well suited to describe the charging dynamics, and will be used for further data analysis. All Ag^{z+} with $z \geq 3$ show a similar general behavior: for optical delays around $\Delta t = 0\,\mathrm{ps}$ the yields exhibit a distinct minimum. With increasing delay the ion signals rise strongly. Each fragment channel shows a pronounced optimum which appears to be rather sharp. Only for the singly and doubly charged ions (not plotted in Fig. 2) the dual-pulse signal exhibits an additional enhancement around zero delay, which can be attributed to direct optical field ionization due to constructive interference of both laser pulses giving an up to fourfold increase in the peak intensity.

In order to achieve a better understanding of the ionization dynamics we make use of the fitting procedure according to equation (2), see also inset of Figure 3. For each z the optimum delay $\Delta t_M(z)$ and the width of the maximum $\delta t(z)$ are extracted from the fit curves, see Figure 3. Obviously both quantities turn out to be a function of z, i.e. they decrease to higher z and finally converge to a finite value. The most intuitive quantity is $\Delta t_M(z)$ being the optical delay which maximizes the count rate of Ag^{z+}

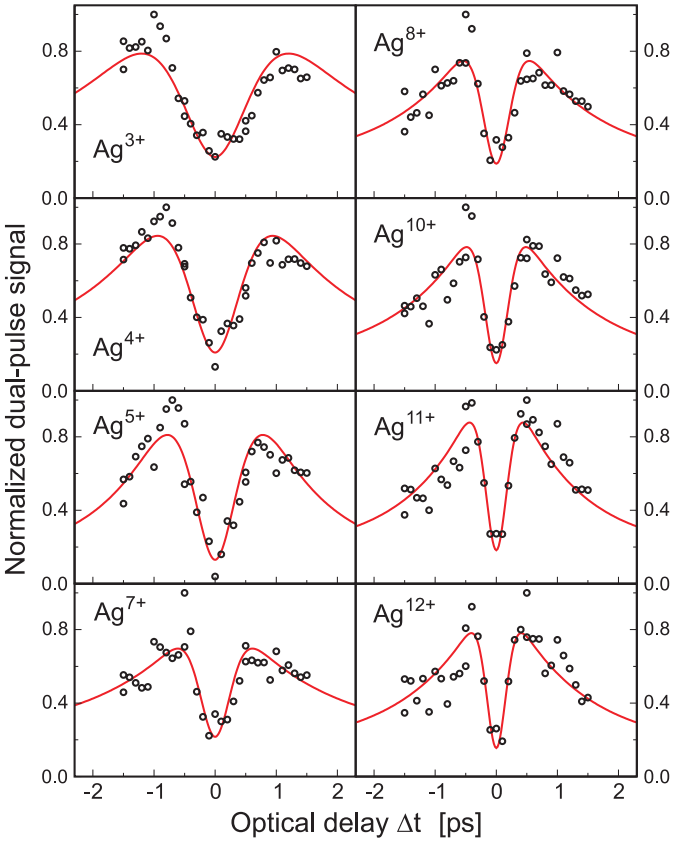

Fig. 2. Dual-pulse signals of selected decay channels resulting from the Coulomb explosion of Ag clusters ($\overline{N} = 80$) after excitation by 800 nm laser light pulses with an energy of 2.5 mJ and a width of $\tau = 100\,\mathrm{fs}$. Focussing the light yields a peak intensity of $5.2\times10^{15}\,\mathrm{W/cm^2}$. The data points (circles) are fitted by equation (2) assuming identical laser pulses. The fit curves (solid lines) will be used for analyzing the charging dynamics.

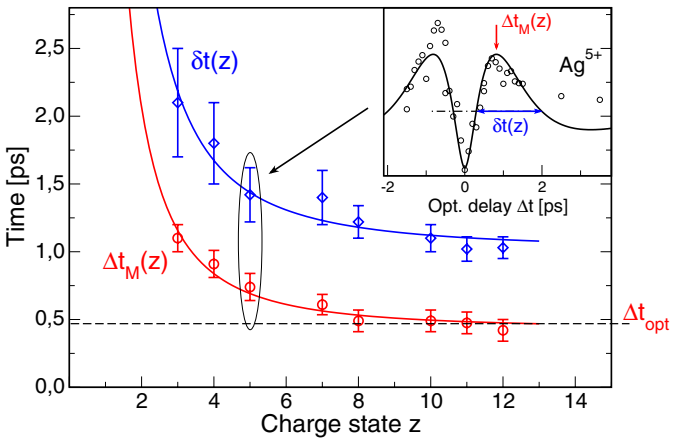

Fig. 3. Charge state selective analysis of the dual-pulse signals. The values are extracted from the fit curves in Figure 2. The definition of the physical quantities $\Delta t_M(z)$ (circles) and $\delta t(z)$ (diamonds) is shown in the inset. Note, that for high charge states the optimum delay converges to a level which we define as Δt_{opt} (dashed line). The data points were fitted to a $1/z^2$ function which serves as a guide to the eye only.

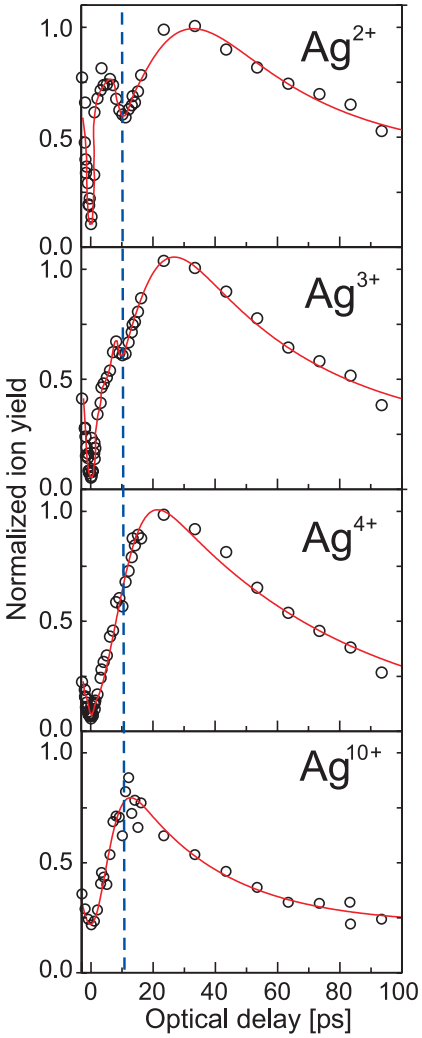

Fig. 4. As Figure 2 but now for a peak intensity of 2.5×10^{13} W/cm^2 and Ag_N with a mean cluster radius of 4.5 nm ($\overline{N}$ = 22000 atoms). For low-z ions an additional feature appears at about 10 ps which is marked by the vertical dashed line.

at the detector. We define the high-z limit of $\Delta t_M(z)$ as Δt_{opt}, illustrated by the dashed line in Figure 3. This is the optical delay leading to the maximum yield of the highest charged ions at the detector and turns out to be 470 fs for the chosen experimental conditions. $\delta t(z)$ is defined as the width (FWHM) of the peak centered at $\Delta t_M(z)$. It's value is mainly determined by the cluster size distribution, the spatial laser intensity profile, and also by the frequency range in which resonant excitation is possible. As an additional feature the dip width around zero delay could be analyzed. In most experiments it turns out to coincide with $\Delta t_M(z)$. In the next section we will investigate the influence of the laser intensity on the charging dynamics by means of $\Delta t_M(z)$. The dependence of Δt_M and δt on z will be discussed in Section 4.2.

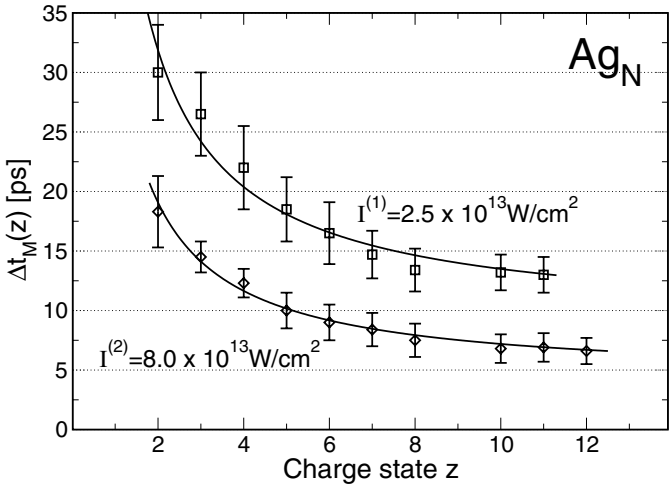

Fig. 5. Charge specific optimum optical delays $\Delta t_M(z)$ for dual-pulse excitation of large silver clusters ($\overline{r}$ = 4.5 nm) at two different laser intensities. The dual-pulse signals for the lower laser intensity partially are shown in Figure 4. The data points are fitted with a $1/z$ function.

3.2 Laser intensity dependence

Having found that Δt_M varies with the charge state z it is interesting to study how the laser intensity influences the charging process in detail. In order to achieve an improved time resolution additional measurements were performed on significantly larger clusters. For rare gas clusters it was shown that large systems expand slower than small ones [34], leading to a delayed plasmon enhanced ionization. In our experiment, by choosing clusters with a mean number of $\overline{N}$ = 22000 silver atoms ($\overline{r}$ = 4.5 nm) as well as a reduced laser intensity we are able to lengthen the time scale in a dual-pulse experiment by more than one order of magnitude from the femtosecond up into the picosecond regime. As an example, Figure 4 shows the resulting yield of selected Ag^{z+} ions at a laser peak intensity of 2.5×10^{13} W/cm^2. Under these conditions a variation in the dual-pulse signals is apparent up to optical delays of more than 100 ps. Note, that an additional structure appears on the left hand side of the maximum for the low ionization states, i.e. Ag^{2+}, Ag^{3+} and, not significantly, for Ag^{4+}. The corresponding dip is marked by the dashed vertical line. This feature appears for certain experimental parameters which, up to now, do not show a systematic pattern. A possible interpretation will be discussed in Section 4.3.

Figure 5 shows the values for $\Delta t_M(z)$ which were obtained from the signals in Figure 4 and from an experiment with a higher laser intensity at 8×10^{13} W/cm^2. For both measurements the general trend of $\Delta t_M(z)$ is the same as for the experiment analyzed in Figure 3, i.e. $\Delta t_M(z)$ decreases with z. In addition, a clear influence of the laser intensity can be observed. First, for each charge state, $\Delta t_M(z)$ is lower for the higher intensity. Also, the optimum optical delay is reduced from $\Delta t_{opt}^{(1)}$ = 13.5 ps for $I^{(1)} = 2.5\times10^{13}$ W/cm^2 to $\Delta t_{opt}^{(2)}$ = 5.5 ps in the case of

$I^{(2)} = 8.0 \times 10^{13}\,\mathrm{W/cm^2}$. Secondly, the higher laser intensity leads to higher z-values. This is reflected in the observed maximum charge state, which increases from $z^{(1)}_{max} = 11$ to $z^{(2)}_{max} = 12$. We emphasize that for Ag^{11+} the $5d$ shell is completely emptied. The next ionization step requires considerably more energy, i.e. 270 eV compared to 190 eV for the ionization of Ag^{10+}. In addition, at optimum delay the absolute count rate of highly charged ions also rises with intensity, e.g., for Ag^{11+} from 0.13 to 0.51 events per laser shot. Note, that in the higher intensity measurement most likely even higher charged ions are generated, but can not be identified due to the signal from residual gas, see Figure 1.

4 Discussion

4.1 Semiclassical simulations

In order to illustrate the basic physical mechanism which is responsible for the charging enhancement we have performed numerical simulations on the model system Na_{55}. The cluster is irradiated by a sequence of two 50 fs laser pulses with an intensity of $4{\times}10^{12}\,\mathrm{W/cm^2}$, see Figure 6a. The first pulse which is centered at a model time of 100 fs interacts with the cluster in its ground state geometry corresponding to a non-resonant excitation. As a result only a small dipole amplitude is induced (Fig. 6b) and four electrons are released from the cluster (Fig. 6c). Due to the ionization and weak thermal excitation the cluster is unstable and starts to expand, see full line in Figure 6d. To investigate the role of the ionic motion on the charging of the cluster performed by the second pulse an additional scenario with fixed ionic positions is considered (dashed lines in Figs. 6c and 6d). With unconstrained propagation the cluster radius increases and reaches a critical value R_c which allows for a resonant excitation of the dipole-plasmon. A rough estimate of R_c can be obtained from the Mie formula (Eq. (1)) as

$$R_c = R_o(\omega_o/\omega_L)^{2/3} \qquad (3)$$

with R_o the initial cluster radius and $\hbar\omega_o$ the plasmon energy in the ground state. For the given example the critical radius of about $1.5R_o$ is attained at a model time of 350 fs, see dotted line in Figure 6d. Feeding in the second pulse at that particular delay results in a significantly larger amplitude of the dipole signal for the scenario with full ionic propagation. This indicates a much stronger coupling compared to the first pulse and in particular to the calculation with fixed ionic geometry (Fig. 6b).

Further support for resonant excitation is given by the phase Φ between the driving laser field and the dipole moment (not shown here). While the cluster radius is approaching R_c, Φ increases from about zero to $\pi/2$. The phase lag of $\Phi = \pi/2$ which is a clear sign for a resonant excitation process is not present in the fixed geometry scenario. As a result of the plasmon excitation not only the dipole amplitude but also the energy absorption increases which is reflected in the degree of ionization, see Figure 6c.

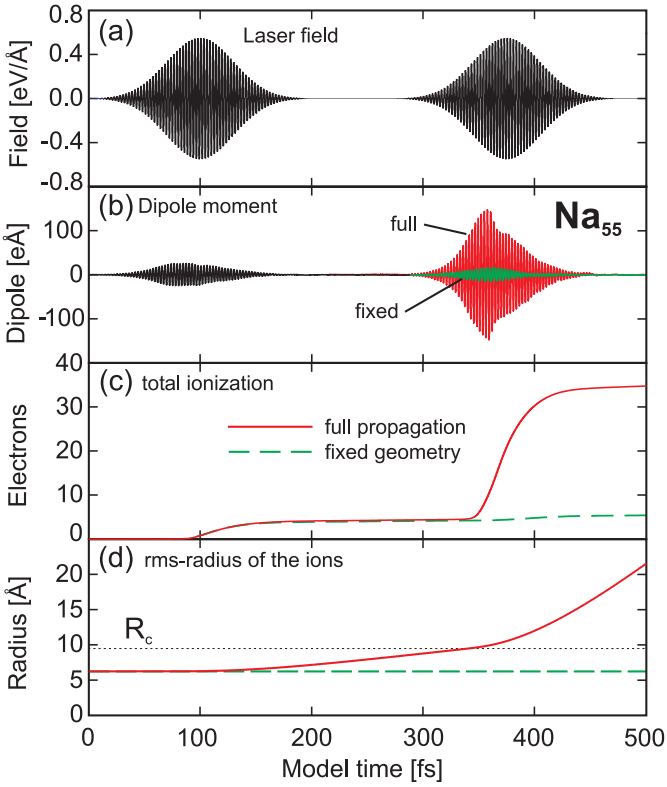

Fig. 6. Response of Na_{55} when irradiated with two 50 fs laser pulses of $4{\times}10^{12}\,\mathrm{W/cm^2}$ which are separated by 275 fs. From top to bottom: (a) laser field strength, (b) dipole response, (c) number of emitted electrons and (d) cluster radius. In the case of the fixed ion geometry the dipole response during the second pulse is strongly reduced, resulting in a considerably lower final ionization of the cluster, see dashed line in (c).

The final number of emitted electrons reaches 35 which is sevenfold higher compared to fixed geometry conditions. Whereas in the unconstrained simulation the second pulse has by far the highest impact on the ionization, it actually releases less electrons compared to the first pulse in the scenario with rigid ions.

The simulations give clear evidence that the charging process can be divided into two steps, and that the initial ionic motion is necessary to "prepare" the enhanced ionization. The first pulse causes the initial charging by OFI, i.e. the intensity of the first pulse is responsible for the time scale of the charging process, see Figure 5. The second pulse when applied with the correct delay for resonant excitation then determines the final degree of ionization, i.e. the higher its intensity the higher the maximum charge state. These relations have also been confirmed in experiments with dual-pulses of different intensities.

Quantitative differences between the simulations and the experiments result from the fact that the simulations were performed on the model system Na_{55}, treating only one valence electron explicitly, i.e. a maximum of 55 electrons can be released from the cluster. Therefore the laser intensity has to be reduced compared to the experiments to avoid saturation effects. So far the semiclassical

simulations are able to describe the main physical mechanisms of the response of metal clusters to moderate laser fields. For higher intensities resonant coupling is expected to be effective even for more active electrons although the peak of the dipole amplitude might be reduced due to collisional damping [23].

4.2 Charge state dependence of Δt_M

In the following we concentrate on the dependence of Δt_M on z, but the arguments also hold for δt. The results shown in Figures 3 and 5 reveal that for each atomic ionization state a different optical delay is required in order to maximize its yield, i.e. the maximization of lower charge states requires larger Δt_M. This phenomenon can be explained by the variation of the laser intensity in the focus which can reach several orders of magnitude. Therefore an experiment is always carried out for different laser intensities simultaneously, and the resulting ions are indistinguishably mapped onto the detector. Hence the charging dynamics depends on the position of the particle within the interaction region. For an illustration we concentrate on clusters in the outer focus region. Due to the lower laser intensity the initial charging via OFI is reduced leading to a slower expansion of the system compared to clusters located closer to the center of the focus. The critical radius R_c is therefore reached later in time and hence Δt_M increases. Moreover, even at resonance the reduced laser intensity lowers the amount of energy which can be coupled into the system. The final charge state is thus lower compared to clusters closer to the center of the laser focus. In summary, the farther away from the center of the laser focus, the longer the time of the charging process, i.e. Δt_M, and the lower the final ionization state of the cluster.

Additional support for this argumentation stems from the volumetric effect induced by the focussing, i.e. the interaction volume increases exponentially to lower laser intensities [35]. This should be reflected in the absolute number of ions collected from the different focus regions. Indeed, the signal for a certain charge state z measured at $\Delta t_M(z)$ decreases roughly exponentially with z, i.e. the lowly charged ions are dominantly collected from the outer focus regions whereas the highly charged ions originate from the center of the focus.

4.3 Saturation effects at resonance

In addition to the charge state dependent shift of $\Delta t_M(z)$ the dual-pulse signals shown in Figure 4 reveal an additional structure. For the low-z ions on the left hand side of the main peak a shoulder is present followed by a dip at about 10 ps. This feature might be due to the most effective absorption of laser radiation into the clusters at this particular optical delay, i.e. the excitation occurs exactly at the resonance condition. As a result, a substantial fraction of particles within the interaction volume is ionized to a high degree yielding a notably decrease of the low-z ion signal. Note, that as a function of the ionization state the value of $\Delta t_M(z)$ approaches the position of the low-z dip (see dashed line in Fig. 4), which independently confirms the suggested underlying process. The width of the dip is apparently smaller than δt of the high-z species which are analyzed in the measurement. One could presume, that the depression of the yield obtained for Ag^{2+} and Ag^{3+} is an image of the dual-pulse signal of the most highly charged fragment ions ($z \geq 12$), the signal of which might not fully be recorded due to the contribution from the residual gas.

The presence of this additional feature strongly depends on the experimental conditions. Up to now the critical parameters couldn't satisfactorily be identified. Possibly this effect can only be observed clearly in a narrow laser intensity range. Experiments are under way in order to clarify this issue.

5 Conclusion

The charging of free silver clusters in strong laser fields has been studied by dual-pulse excitation over a broad cluster size range. Depending on the laser intensity and the cluster size, an optical delay between 0.45 ps and 13.5 ps is necessary in order to drive the plasmon mode of the cluster into resonance with the laser field and allow for an effective charging of the system. The optimum time delay to reach maximum charging, Δt_{opt}, scales with the cluster size and inversely with the laser intensity. For the maximization of certain ionic charge states different optical delays have to be applied which can be explained by the sampling over a broad laser intensity range in the interaction region. This may open a possible route to drive the VUV-emission of clusters towards a preselected value, e.g. 13 nm which will be used by the next generation lithography.

Financial support by the Deutsche Forschungsgemeinschaft through the SFB 652 (*Strong correlations and collective effects in radiation fields: Coulomb systems, clusters and particles*) is gratefully acknowledged.

References

1. M. Lezius, S. Dobosz, D. Normand, M. Schmidt, Phys. Rev. Lett. **80**, 261 (1998)
2. T. Ditmire, J.W.G. Tisch, E. Springate, M.B. Mason, N. Hay, R.A. Smith, I. Marangos, M.M.R. Hutchinson, Nature **386**, 54 (1997)
3. V. Kumarappan, M. Krishnamurthy, D. Mathur, Phys. Rev. A **66**, 033203 (2002)
4. A. McPherson, B.D. Thompson, A.B. Borisov, K. Boyer, C.K. Rhodes, Nature **370**, 631 (1994)
5. T. Ditmire, J. Zweiback, V.P. Yanovsky, T.E. Cowan, G. Hays, K.B. Wharton, Nature **398**, 489 (1999)
6. T. Ditmire, R.A. Smith, J.W.G. Tisch, M.H.R. Hutchinson, Phys. Rev. Lett. **78**, 3121 (1997)
7. E. Parra, I. Alexeev, J. Fan, K.Y. Kim, S.J. McNaught, H.M. Milchberg, Phys. Rev. E **62**, R7603 (2000)

8. M. Schnürer, S. Ter-Avetisyan, H. Stiel, U. Vogt, W. Radloff, M. Kalashnikov, W. Sandner, P.V. Nickles, Eur. Phys. J. D **14**, 331 (2001)
9. S. Düsterer, H. Schwoerer, W. Ziegler, D. Salzmann, R. Sauerbrey, Appl. Phys. B **76**, 17 (2003)
10. D. Attwood, *Soft X-rays and extreme ultraviolet radiation* (Cambridge University Press, 1999)
11. H. Wabnitz, L. Bittner, A.R.B. de Castro, R. Döhrmann, P. Gürtler, T. Laarmann, W. Laasch, J. Schulz, A. Swidarski, K. von Haeften, T. Möller, B. Faatz, A. Fateev, J. Feldhaus, C. Gerth, U. Hahn, E. Saldin, E. Schneidmiller, K. Sytchev, K. Tiedtke, R. Treusch, M. Yurkov, Nature **420**, 482 (2002)
12. R. Santra, C.H. Greene, Phys. Rev. Lett. **91**, 233401 (2003)
13. Ch. Siedschlag, J.-M. Rost, Phys. Rev. Lett. **93**, 043402 (2004)
14. *Metal clusters*, edited by W. Ekardt (John Wiley & Sons Ltd., Chichester, 1999)
15. G. Mie, Ann. Phys. **25**, 377 (1908)
16. W.A. de Heer, Rev. Mod. Phys. **65**, 611 (1993)
17. J. Tiggesbäumker, L. Köller, K.-H. Meiwes-Broer, A. Liebsch, Phys. Rev. A **48**, R1749 (1993)
18. T. Ditmire, T. Donnelly, A.M. Rubenchik, R.W. Falcone, M.D. Perry, Phys. Rev. A **53**, 3379 (1996)
19. L. Köller, M. Schumacher, J. Köhn, S. Teuber, J. Tiggesbäumker, K.-H. Meiwes-Broer, Phys. Rev. Lett. **82**, 3783 (1999)
20. J. Daligault, C. Guet, Phys. Rev. A **64**, 043203 (2001)
21. Th. Fennel, K.-H. Meiwes-Broer, G.F. Bertsch, Eur. Phys. J. D **29**, 367 (2004)
22. E. Suraud, P.G. Reinhard, Phys. Rev. Lett. **85**, 2296 (2000)
23. U. Saalmann, J.-M. Rost, Phys. Rev. Lett. **91**, 223401 (2003); Ch. Siedschlag, J.-M. Rost, Phys. Rev. A **71**, 031401R (2005)
24. C. Rose-Petruck, K.J. Schäfer, K.R. Wilson, C.P.J. Barty, Phys. Rev. A **55**, 1182 (1997)
25. Ch. Siedschlag, J.-M. Rost, Phys. Rev. A **67**, 013404 (2003)
26. T. Seidemann, M.Yu. Ivanov, P.B. Corkum, Phys. Rev. Lett. **75**, 2819 (1995)
27. E. Springate, S.A. Aseyev, S. Zamith, M.J.J. Vrakking, Phys. Rev. A **68**, 053201 (2003)
28. T. Döppner, Th. Fennel, Th. Diederich, J. Tiggesbäumker, K.-H. Meiwes-Broer, Phys. Rev. Lett. **94**, 013401 (2005)
29. H. Haberland, M. Mall, M. Moseler, Y. Qiang, T. Reiners, Y. Thurner, J. Vac. Sci. Technol. A **12**, 2925 (1994)
30. P. Radcliffe, T. Döppner, S. Teuber, M. Schumacher, J. Tiggesbäumker, K.-H. Meiwes-Broer, Contrib. Plasm. Phys. **45**, 424 (2005)
31. B.A. Mamyrin, V.I. Karataev, D.V. Shmikk, V.A. Zagulin, Rev. Sci. Instr. **37**, 45 (1973)
32. S. Teuber, T. Döppner, T. Fennel, J. Tiggesbäumker, K.-H. Meiwes-Broer, Eur. Phys. J. D **16**, 59 (2001)
33. L. Plagne, J. Daligault, K. Yabana, T. Tazawa, Y. Abe, C. Guet, Phys. Rev. A **61**, 33201 (2000)
34. J. Zweiback, T. Ditmire, M.D. Perry, Phys. Rev. A **59**, R3166 (1999)
35. P. Hansch, M.A. Walker, L.D. Van Woerkom, Phys. Rev. A **54**, R2559 (1996)